

Deciphering signatures of Bardeen black holes from the observed quasi-periodic oscillations

Indrani Banerjee*¹

¹Department of Physics and Astronomy, National Institute of Technology, Rourkela-769008, India

Abstract

Quasi-periodic oscillations (QPOs) observed in the power spectrum of black holes are unique observational probes to the background spacetime since they can be directly related to the timescales associated with the motion of matter orbiting in the vicinity of the black hole horizon. In this regard, the high frequency QPOs (HFQPOs) are particularly interesting as they occur in commensurable pairs, the most common ratio being the 3:2 twin peak QPOs. The theoretical models which aim to explain these QPOs express the observed frequencies in terms of the epicyclic motion of test particles in a given background spacetime. In this work we study the signatures of Bardeen spacetime from the observed QPOs in the black hole power spectrum. Bardeen black holes are rotating, regular black holes with a magnetic monopole charge. Such regular backgrounds are theoretically interesting as they can potentially evade the curvature singularity, otherwise unavoidable in general relativistic black holes. We perform a χ^2 analysis by comparing the available observations of the quasi-periodic oscillations from black hole sources with the relevant theoretical models and note that the Kerr black holes in general relativity are observationally more favored compared to black holes with a monopole charge. Our analysis reveals that black holes with very high monopole charge are *disfavored* from QPO related observations.

1 Introduction

Despite the astounding success of general relativity in explaining a plethora of observations, e.g. perihelion precession of mercury, bending of light, gravitational redshift [1–4], black hole image [5–11] and gravitational waves [12–16], there remains certain unresolved issues in both observational and theoretical fronts. In the observational end it cannot address adequately the dark sector [17–22] while in the theoretical front general relativity still cannot explain the big bang and black hole singularities [23–26]. In this regard, study of regular black holes is important as it can provide a possible resolution to the black hole singularity problem. Regular black holes arise in several alternative gravity theories, one such scenario being study of Einstein gravity in presence of non-linear electrodynamics. In this regard we study Bardeen black holes [27], which correspond to black hole with a magnetic monopole charge.

In order to investigate observational signatures of Bardeen metric we consider quasi-periodic oscillations (QPOs) observed in the power spectrum of black holes [28, 29]. In particular, the high frequency quasi-periodic oscillations (HFQPOs) are interesting as these can be used to decipher the nature of the background spacetime. This is because, the observed frequency range of QPOs varies from mHz (for supermassive black

*banerjeein@nitrkl.ac.in

holes) to hundreds of Hz (for stellar-mass black holes) which in turn is associated with dynamical timescales ($\sim 0.1\text{--}1$ ms) of motion of accreting matter very close to the black hole event horizon. One can heuristically derive such dynamical timescales $t_d \sim \sqrt{(r^3/GM)}$ from characteristic velocities $v \sim \sqrt{(GM/r)}$ of motion of accreting matter near the central object. Considering, $r \sim 100$ km for a $10 M_\odot$ black hole, the dynamical timescale turns out to be $t_d \sim 1$ ms. This estimation shows that the dynamical timescales are in the millisecond range, predicted back in the 1970s [30, 31] and received observational confirmation with the launch of NASA's Rossi X-Ray Timing Explorer satellite [28].

Several theoretical models exist in the literature which aims to explain these observed HFQPOs. These requires one to study the epicyclic motion of test particles around these compact objects. The theoretically predicted QPO frequencies in all of these models turn out to be linear combinations of the angular frequency and the epicyclic frequencies. In next section we discuss the Bardeen black hole solution, i.e. Einstein gravity in non-linear electrodynamics. In Section 3 we derive the epicyclic frequencies in a general stationary axisymmetric spacetime. The existing QPO models are briefly discussed in Section 4. In Section 5 we compare the theoretical QPO frequencies obtained from each of these models with the available observations. We perform a χ^2 analysis to derive the observationally favored magnetic monopole charge parameter. We conclude with a summary of our results with some scope for future work in Section 6. It may be important to note that we work with mostly positive metric convention and consider geometrized units i.e., $G = 1 = c$.

2 Basics of Bardeen rotating black holes

The line element corresponding to Bardeen black hole [27] in Boyer-Lindquist coordinates is given by,

$$ds^2 = -\left(1 - \frac{2\tilde{m}(r)r}{\tilde{\Sigma}}\right)dt^2 - \frac{4a\tilde{m}(r)r}{\tilde{\Sigma}}\sin^2\theta dt d\phi + \frac{\tilde{\Sigma}}{\Delta}dr^2 + \tilde{\Sigma}d\theta^2 + \left(r^2 + a^2 + \frac{2\tilde{m}(r)ra^2}{\tilde{\Sigma}}\sin^2\theta\right)\sin^2\theta d\phi^2 \quad (1)$$

where,

$$\tilde{\Sigma} = r^2 + a^2 \cos^2\theta, \quad \Delta = r^2 + a^2 - 2\tilde{m}(r)r \quad (2)$$

and $\tilde{m}(r)r$ is the mass function such that $\lim_{r \rightarrow \infty} \tilde{m}(r) = \tilde{\mathcal{M}}$ and a is the Kerr parameter. The mass function corresponding to the Bardeen rotating black hole is given by,

$$\tilde{m}(r) = \tilde{\mathcal{M}} \left[\frac{r^2}{r^2 + \tilde{g}^2} \right]^{3/2} \quad (3)$$

where \tilde{g} is the magnetic monopole charge. Due to the presence of the magnetic monopole charge Bardeen black hole has no curvature singularity, i.e., spacetime is regular everywhere and it satisfies the weak energy condition.

The black hole solution corresponding to Eq. (1) arises in nonlinear electrodynamics [27], the associated action being given by,

$$\mathcal{S} = \int d^4x \left[\frac{\mathcal{R}}{16\pi} - \frac{\mathcal{W}(f)}{4\pi} \right] \quad (4)$$

In Eq. (4) \mathcal{R} is the Ricci scalar, $\mathcal{W}(f)$ is a function of $f = \frac{1}{4}\mathcal{F}_{\mu\nu}\mathcal{F}^{\mu\nu}$ where $\mathcal{F}_{\mu\nu} = 2\nabla_{[\mu}A_{\nu]}$ as the electromagnetic field strength. Varying the above action with respect to the metric we obtain the following gravitational field equations:

$$\mathcal{G}_\mu^\nu = 2\left[\mathcal{W}_f(\mathcal{F}_{\mu\lambda}\mathcal{F}^{\nu\lambda}) - \delta_\mu^\nu\mathcal{W}\right] \quad (5)$$

$$\nabla_\mu(\mathcal{W}_f\mathcal{F}^{\beta\mu}) = 0 \quad (6)$$

with $\mathcal{W}_f = \frac{\partial\mathcal{W}}{\partial f}$. For Bardeen spacetime the form of \mathcal{W}_f is given by,

$$\mathcal{W}(f) = \frac{3\mathcal{M}}{|\tilde{g}|\tilde{g}^2}\left[\frac{\sqrt{2\tilde{g}^2f}}{1 + \sqrt{2\tilde{g}^2f}}\right]^{5/2} \quad (7)$$

It is important to note that Kerr black hole can be retrieved in the absence of nonlinear electrodynamics i.e $\tilde{g} = f = 0$. We aim to constrain both the parameters a and \tilde{g} in the light of astrophysical observations.

In order to calculate the event horizon corresponding to the above spacetime we put $g^{rr} = \Delta = 0$ which gives,

$$r^2 + a^2 - 2\mathcal{M}r\left(\frac{r^2}{r^2 + \tilde{g}^2}\right)^{3/2} = 0 \quad (8)$$

We require real and positive solutions of the above equation which enables us to understand the observationally favored magnetic monopole charge parameter \tilde{g} . Henceforth, in this paper we will denote the magnetic monopole charge by $g = \tilde{g}^2$. In the next section we discuss how to derive the luminosity from the accretion disk in the Bardeen spacetime.

3 Epicyclic frequencies of test particles in a stationary axisymmetric black hole spacetime

In this section we study the motion of massive test particles around a rotating black hole which is described by a stationary, axisymmetric spacetime possessing reflection symmetry. The metric around such a black hole is given by,

$$ds^2 = g_{tt}dt^2 + 2g_{t\phi}dtd\phi + g_{\phi\phi}d\phi^2 + g_{rr}dr^2 + g_{\theta\theta}d\theta^2, \quad (9)$$

such that $g_{\alpha\beta} = g_{\alpha\beta}(r, \theta)$ and $g_{\mu\nu}(r, \theta) = g_{\mu\nu}(r, -\theta)$. It is clear from Eq. (9) that the above spacetime has two Killing vectors namely ∂_t and ∂_ϕ such that the specific energy E and the specific angular momentum L of the test particles are conserved. One can show from the invariance of the rest mass of the test particles that,

$$\dot{r}^2g_{rr} + \dot{\theta}^2g_{\theta\theta} + E^2U(r, \theta) = -1 \quad (10)$$

where $U(r, \theta) = (g^{tt} - 2lg^{t\phi} + l^2g^{\phi\phi})$ corresponds to the effective potential due to the central black hole in which the test particles moves and $l = L/E$ is the impact parameter. We first consider circular equatorial motion of the test particles such that $E^2U(r_0, \pi/2) = -1$ where r_0 corresponds to the radius of the circular orbit.

The angular frequency corresponding to the circular, equatorial motion of test particles in the above background is obtained by solving the equation,

$$g_{tt,r} + 2\Omega g_{t\phi,r} + \Omega^2 g_{\phi\phi,r} = 0 . \quad (11)$$

such that

$$\Omega = \frac{-g_{t\phi,r} \pm \sqrt{g_{t\phi,r}^2 - g_{tt,r}g_{\phi\phi,r}}}{g_{\phi\phi,r}} \quad (12)$$

where \pm sign corresponds to prograde and retrograde orbits. We now consider slight perturbation in the motion of the test particle from the circular orbit and the equatorial plane. Let us denote this by,

$$r(t) \simeq r_0 + \delta r_0 e^{i\omega_r t} ; \quad \theta(t) \simeq \frac{\pi}{2} + \delta\theta_0 e^{i\omega_\theta t} . \quad (13)$$

where ω_r and ω_θ correspond to radial and vertical epicyclic frequencies respectively. Substituting Eq. (13) in Eq. (10) and Taylor expanding $U(r, \theta)$ about $r = r_0$ and $\theta = \pi/2$,

$$-\delta r_0^2 \omega_r^2 (u^t)^2 g_{rr} - \delta\theta_0^2 \omega_\theta^2 (u^t)^2 g_{\theta\theta} + E^2 \left[U(r_0, \pi/2) + \frac{1}{2} \frac{\partial^2 U}{\partial r^2} \Big|_{r=r_0, \theta=\pi/2} \delta r_0^2 + \frac{1}{2} \frac{\partial^2 U}{\partial \theta^2} \Big|_{r=r_0, \theta=\pi/2} \delta\theta^2 \right] = -1 \quad (14)$$

We have noted earlier that $E^2 U(r_0, \pi/2) + 1 = 0$ and since the motion along the radial and the vertical direction are uncoupled in the linear approximation we may equate the coefficients of δr^2 and $\delta\theta^2$ on both sides of Eq. (14). This yields the following expressions for the radial and the vertical epicyclic frequencies:

$$\omega_r^2 = \frac{c^6}{G^2 M^2} \frac{(g_{tt} + \Omega g_{t\phi})^2}{2g_{rr}} \frac{\partial^2 U}{\partial r^2} \Big|_{r=r_0, \theta=\pi/2} \quad (15)$$

$$\omega_\theta^2 = \frac{c^6}{G^2 M^2} \frac{(g_{tt} + \Omega g_{t\phi})^2}{2g_{\theta\theta}} \frac{\partial^2 U}{\partial \theta^2} \Big|_{r=r_0, \theta=\pi/2} \quad (16)$$

The radial and vertical epicyclic frequencies are multiplied by the factor $(c^6/G^2 M^2)$ so that they have dimensions of frequency squared.

We next discuss various theoretical models aimed to explain the observed high frequency quasi-periodic oscillations (HFQPOs) in the power spectrum of black holes. HFQPOs are observed in some stellar mass black holes and supermassive black holes with frequencies \sim hundreds of Hz and \sim mHz respectively [32–34]. The order of magnitude of these QPO frequencies can be directly attributed to the masses of the black hole in question (see Eq. (16)). Apart from the HFQPOs, some of these black holes also exhibit low frequency QPOs (LFQPOs) in their power spectrum. In Table 1 we present a few BH sources where QPOs have been discovered. Interestingly, it turns out that the HFQPOs in the BH sources appear generally in the ratio of 3:2. The two observed HFQPOs are denoted by f_{u1} and f_{u2} while the low frequency QPO is denoted by f_L . In this regard it may be important to note that the RE J1034+396 galaxy exhibits only a single QPO in its power spectrum [32, 35–37].

Various theoretical models have been proposed to explain the observed QPOs in the black hole power spectrum [38–54]. These models chiefly aim to explain the commensurability of the QPO frequencies. The theoretical HFQPOs obtained from various models are denoted by f_1 and f_2 while the theoretical low

frequency QPO is denoted by f_3 . The mathematical expressions for each of these QPO frequencies from various QPO models are presented in Table 2 from which it is evident that these QPO frequencies are linear combinations of ν_ϕ , ν_r and ν_θ . It may be important to note that the theoretical QPO frequencies depend solely on the background spacetime and not on the complex physics of the accretion processes. Therefore, QPOs can potentially be a cleaner probe to the background spacetime compared to other available observations, e.g., the iron line or the continuum-fitting methods. Further, we will consider only those sources in Table 1 (namely, the first five sources) which exhibit the 3:2 ratio HFQPOs. Therefore the data related to RE J1034+396 galaxy will not be used for subsequent analysis.

In the present work we assume the black holes mentioned in Table 1 to be Bardeen BHs and aim to extract their magnetic monopole charge from QPO related observations.

Source	Mass (in M_\odot)	$f_{u1} \pm \Delta f_{u1}$ (in Hz)	$f_{u2} \pm \Delta f_{u2}$ (in Hz)	$f_L \pm \Delta f_L$ (in Hz)
GRO J1655 – 40	5.4 ± 0.3 [55]	441 ± 2 [56]	298 ± 4 [56]	17.3 ± 0.1 [56]
XTE J1550 – 564	9.1 ± 0.61 [57]	276 ± 3	184 ± 5	–
GRS 1915 + 105	$12.4^{+2.0}_{-1.8}$ [58]	168 ± 3	113 ± 5	–
H 1743 + 322	$8.0 - 14.07$ [59–61]	242 ± 3	166 ± 5	–
Sgr A*	$(3.5 - 4.9) \times 10^6$ [62, 63]	$(1.445 \pm 0.16) \times 10^{-3}$ [33, 64]	$(0.886 \pm 0.04) \times 10^{-3}$ [33, 64]	–
REJ1034 + 396	$(1 - 4) \times 10^6$ [32, 65–67]	$(2.5 - 2.8) \times 10^{-4}$ [32, 35–37]	–	–

Table 1: Black hole sources exhibiting high frequency QPOs (HFQPOs)

Model	f_1	f_2	f_3
Relativistic Precession Model (kinematic) [38–40]	ν_ϕ	$\nu_\phi - \nu_r$	$\nu_\phi - \nu_\theta$
Tidal Disruption Model (kinematic) [41–43]	$\nu_\phi + \nu_r$	ν_θ	–
Parametric Resonance Model (resonance) [44–46]	ν_θ	ν_r	–
Forced Resonance Model 1 (resonance) [44]	ν_θ	$\nu_\theta - \nu_r$	–
Forced Resonance Model 2 (resonance) [44]	$\nu_\theta + \nu_r$	ν_θ	–
Keplerian Resonance Model 1 (resonance) [47]	ν_ϕ	ν_r	–
Keplerian Resonance Model 2 (resonance) [47]	ν_ϕ	$2\nu_r$	–
Keplerian Resonance Model 3 (resonance) [47]	$3\nu_r$	ν_ϕ	–
Warped Disk Oscillation Model (resonance)	$2\nu_\phi - \nu_r$	$2(\nu_\phi - \nu_r)$	–
Non – axisymmetric Disk Oscillation Model 1 (resonance)	ν_θ	$\nu_\phi - \nu_r$	–
Non – axisymmetric Disk Oscillation Model 2 (resonance) [48–50]	$2\nu_\phi - \nu_\theta$	$\nu_\phi - \nu_r$	–

Table 2: Theoretical expressions for the HFQPOs and the LFQPO from various QPO models.

4 Theoretical Models explaining quasi-periodic oscillations in the black hole power spectrum

In this section we review some of the existing theoretical models aimed to explain the observed HFQPOs in BHs. Since the model dependent QPO frequencies (Table 2) are linear combinations of ν_ϕ , ν_r and ν_θ , one can easily check that these are functions of the black hole mass M , the radius at which these oscillations are generated r_{em} and the metric parameters (which in this case corresponds to g and a). The QPO models existing in the literature can be broadly classified into two categories, namely the kinematic models and the resonant models. Below we briefly review the basic features of each of these models:

- **Kinematic models:** In kinematic models the origin of QPOs is attributed to the local motion of plasma in the accretion disk. The two most widely used kinematic models are the Relativistic Precession Model (henceforth referred to as RPM) [38, 39] and the Tidal Disruption Model (TDM) [41–43]. The Relativistic Precession Model, originally proposed to explain the twin HFQPOs in neutron star sources is also used to address the HFQPOs observed in black holes [40]. According to this model, the observed upper and lower HFQPOs (denoted by f_{up1} and f_{up2}) corresponds to the orbital angular frequency and the periastron precession frequency such that $f_1 = \nu_\phi$ and $f_2 = \nu_\phi - \nu_r$. This model can also be used to explain the observed LFQPOs in BHs such that f_L is associated with the nodal precession frequency, i.e., $f_3 = \nu_\phi - \nu_\theta$.

Another widely used kinematic model is the Tidal Disruption Model [41–43]. According to this model, the observed modulation of the flux in the power spectrum leading to HFQPOs is attributed to the plasma orbiting the BH which may get tidally stretched by the central object. In this model, the upper and lower HFQPOs are given by $f_1 = \nu_\phi + \nu_r$ and $f_2 = \nu_\phi$ respectively. Thus, the theoretical QPO frequencies in the above kinematic models depend on the black hole hairs g , a , and M along with the radius r_{em} at which these oscillations are generated.

- **Resonant models:** It is interesting to note that the observed twin-peak HFQPOs (f_{u1} and f_{u2}) in BH and NS sources occur in the ratio of 3:2. This may indicate that the QPOs might originate as a result of resonance between various oscillation modes in the accretion disk [44, 68, 69]. In this regard, the resonant models are more suitable to explain the commensurability of the QPO frequencies [49].

In the previous section we assumed that the accreting matter mostly resides in the equatorial plane and gradually inspirals and falls into the central black hole in nearly circular geodesics. Slight perturbations from the circular orbit r_0 and the equatorial plane are denoted by $\delta r = r - r_0$ and $\delta\theta = \theta - \pi/2$ respectively, such that they obey the equations corresponding to two uncoupled simple harmonic oscillators with frequencies ω_r and ω_θ ,

$$\delta\ddot{r} + \omega_r^2 \delta r = 0 ; \quad \delta\ddot{\theta} + \omega_\theta^2 \delta\theta = 0 . \quad (17)$$

where $\omega_r = 2\pi\nu_r$ and $\omega_\theta = 2\pi\nu_\theta$ correspond to the radial and vertical epicyclic frequencies discussed in Section 3. In a more general situation one needs to incorporate non-linear effects due to pressure and dissipation in the accreting fluid [44, 68] which requires adding forcing terms on the right hand side of Eq. (17),

$$\delta\ddot{r} + \omega_r^2 \delta r = \omega_r^2 F_r(\delta r, \delta\theta, \delta\dot{r}, \delta\dot{\theta}) ; \quad \delta\ddot{\theta} + \omega_\theta^2 \delta\theta = \omega_\theta^2 F_\theta(\delta r, \delta\theta, \delta\dot{r}, \delta\dot{\theta}) . \quad (18)$$

In Eq. (18) the forcing terms F_r and F_θ depend non-linearly on their arguments, their explicit forms being dependent on the accretion flow model. Determining the correct analytical forms of F_r and F_θ

is non-trivial since dissipation and pressure effects in accretion physics is not very well understood. However, considering various physical situations different analytical forms for the forces F_r and F_θ are used [45, 70] which gives rise to different resonant QPO models. Below we enlist some of the important resonant QPO models:

1. **Parametric Resonance Model:** According to this model, the radial epicyclic mode induces the vertical epicyclic mode since random fluctuations in thin disks are expected to have $\delta r \gg \delta \theta$ [44–46, 68, 71]. In such a scenario, Eq. (18) assumes the form,

$$\delta \ddot{r} + \omega_r^2 \delta r = 0 \quad \delta \ddot{\theta} + \omega_\theta^2 \delta \theta = -\omega_\theta^2 \delta r \delta \theta \quad (19)$$

From Eq. (19) it can be shown that the equation for $\delta \theta$ is similar to the Mathieu equation [72] describing parametric resonance and is excited when [46, 72]

$$\frac{\nu_r}{\nu_\theta} = \frac{2}{n}, \quad \text{where } n \in \text{positive integers} . \quad (20)$$

Since $\nu_\theta > \nu_r$ [64] for Bardeen black holes, $n = 3$ gives rise to the strongest resonance which in turn naturally explains the observed 3 : 2 ratio of the HFQPOs. Thus, according to this model, $f_1 = \nu_\theta$ and $f_2 = \nu_r$. This finding has been further verified by analytical calculations [46, 70] and numerical simulations [45].

2. **Forced Resonance Models:** In general, accretion flows cannot be always modelled by the thin Keplerian disk [44, 68, 69, 71] due to the presence of pressure, viscous or magnetic stresses prevalent in the accretion flow. This leads to non-linear couplings between δr and $\delta \theta$ in addition to the aforementioned parametric resonance. It has been confirmed from numerical simulations that a resonant forcing of vertical oscillations by radial oscillations can be excited through a pressure coupling [68, 73]. In the absence of an unambiguous understanding of the physics of the accretion flow, such non-linear couplings between δr and $\delta \theta$ are often described by some mathematical ansatz, e.g.,

$$\delta \ddot{\theta} + \omega_\theta^2 \delta \theta = -\omega_\theta^2 \delta r \delta \theta + \mathcal{F}_\theta(\delta \theta) \quad (21)$$

such that $\delta r = A \cos(\omega_r t)$ while \mathcal{F}_θ corresponds to the non-linear terms in $\delta \theta$. One can show that Eq. (21) has solutions of the form,

$$\frac{\nu_\theta}{\nu_r} = \frac{m}{n} \quad \text{where } m \text{ and } n \text{ are natural numbers} \quad (22)$$

We have noted earlier that $m : n = 3 : 2$ is associated with parametric resonance. The presence of non-linear couplings give rise to forced resonances, e.g. $m : n = 3 : 1$ and $m : n = 2 : 1$ which allows resonance between combinations of frequencies, e.g. $\nu_\theta - \nu_r$, $\nu_\theta + \nu_r$.

For 3 : 1 forced resonance model (denoted by Forced Resonance Model 1 or FRM1), the upper HFQPO is given by $f_1 = \nu_\theta$ while the lower HFQPO is given by $f_2 = f_- = \nu_\theta - \nu_r$. In case of 2 : 1 forced resonance model (denoted by Forced Resonance Model 2 or FRM2) $f_1 = f_+ = \nu_\theta + \nu_r$ while $f_2 = \nu_\theta$.

3. **Keplerian Resonance Models:** In Keplerian Resonance Models one considers non-linear resonances between the the orbital angular motion and the radial epicyclic modes [47, 68, 71, 74].

Two possible physical scenarios where such resonances might occur corresponds to: (a) coupling between the radial epicyclic frequencies of a pair of spatially separated coherent vortices with opposite vorticities with their spatially varying orbital angular frequencies [71, 75] and/or (b) trapping of non-axisymmetric g-mode oscillations [74] in the inner parts of relativistic thin accretion disks. It was however shown [76, 77] that the presence of corotation resonance dampens the g-mode oscillations such that Keplerian resonance models may not be very promising in explaining the HFQPOs. Within the purview of the aforementioned scenarios, the Keplerian Resonance may occur between (a) $f_1 = \nu_\phi$ and $f_2 = \nu_r$ (denoted by Keplerian Resonance Model 1 or KRM1), (b) $f_1 = \nu_\phi$ and $f_2 = 2\nu_r$ (denoted by Keplerian Resonance Model 2 or KRM2) and (c) $f_1 = 3\nu_r$ and $f_2 = \nu_\phi$ (which we denoted by Keplerian Resonance Model 3 or KRM3).

4. **Warped Disk Oscillation Model:** This model assumes a somewhat unusual disc geometry [49, 78] and aims to explain the observed HFQPOs by considering non-linear resonances between the relativistic disk deformed by a warp with various disk oscillation modes [79–83]. Such resonances include horizontal resonances inducing g-mode and p-mode oscillations as well as vertical resonances which can induce only the g-mode oscillations [80]. The origin of such resonances can be ascribed to the fact that the radial epicyclic frequency does not exhibit a monotonic variation with the radial distance r [80].
5. **Non-axisymmetric Disk-Oscillation Model:** Non-axisymmetric Disk-Oscillation models are essentially variants of the Relativistic Precession model [49] considering different combinations of non-axisymmetric disc oscillation modes as the origin of the HFQPOs [49, 50, 84–86]. These models include non-geodesic effects in the accretion physics originating from the pressure forces by modelling the accretion flow in terms of a slightly non-slender pressure-supported perfect fluid torus [50, 87, 88].

There exist two main variants of non-axisymmetric disk-oscillation models: the first (denoted by NADO1 or Vertical Precession Resonance Model [84–86]) considers resonance between the vertical epicyclic frequency ($f_1 = \nu_\theta$) with $m = -1$ non-axisymmetric radial epicyclic frequency ($f_2 = \nu_\phi - \nu_r$) while the second (denoted by NADO2) assumes coupling between the $m = -2$ non-axisymmetric vertical epicyclic frequency ($f_1 = 2\nu_\phi - \nu_\theta$) [48–50] with the $m = -1$ non-axisymmetric radial epicyclic frequency ($f_2 = \nu_\phi - \nu_r$). Here m refers to the azimuthal wave number of the non-axisymmetric perturbation.

It is interesting to note that using RPM in Kerr geometry the spin of the microquasar GRO J1655-40 does not agree with the predictions of Continuum Fitting/Fe-line method [56]. However, if NADO1 or Vertical Precession Resonance Model is invoked then the spin of GRO J1655-40 is in agreement with the results obtained from the Continuum Fitting method. However, the physical mechanisms inducing couplings between an axisymmetric and a non-axisymmetric mode or between the pairs non-axisymmetric modes are yet not very well-understood [49, 89].

It is important to note that in the present analysis we have considered only those QPO models where the resonances invoked in the theoretical (model-based) QPO frequencies f_1 and f_2 (and f_3 if included within the purview of the chosen model) occur at the same radial distance r_{em} [50, 78, 90] from the black hole. Such an assumption holds good for the kinematic and resonant models discussed above. Apart from these there also exist another class of models, the so called diskoseismic models, where the oscillatory modes giving rise to the twin HFQPOs are generated at different radii from the accretion disk [51–53]. We shall not consider such models in this work as they cannot suitably explain the observed 3:2 ratio of HFQPOs [91–93].

In the next section we compare the theoretical QPO frequencies obtained from each of the models presented in [Table 2](#) with the available QPO observations in black holes, namely, the first five sources in [Table 1](#). These frequencies depend on the mass of the black hole M , the emission radius r_{em} and the metric parameters g and a . Here, we shall not use the QPO related observations to determine the black hole mass, rather we will consider the mass of these BHs estimated earlier from other independent observations, e.g., optical/NIR photometry (see [Table 1](#)). The errors associated with the observed QPO frequencies are also reported in [Table 1](#). We compute the variation of χ^2 with the monopole charge g corresponding to each of the QPO models. This allows us to discern the most favored magnetic monopole charge within the domain of the QPO models considered.

5 Estimating the magnetic monopole charge from the observed QPOs

In this section we compare the model dependent QPO frequencies enlisted in [Table 2](#) with the observed QPO frequencies in the BH sources. We perform a joint- χ^2 analysis which enables us to decode the observationally favored values of spin a , emission radius r_{em} and the monopole charge parameter g corresponding to each of the BH sources. We emphasize once again that we do not constrain the BH mass from the present analysis but instead use the predetermined masses of these sources from optical/NIR photometry (see [Table 1](#)).

We define the χ^2 function in the following way:

$$\chi^2(g) = \sum_j \frac{\{f_{u1,j} - f_1(g, a_{\min}, M_{\min}, r_{\min})\}^2}{\sigma_{f_{u1},j}^2} + \sum_j \frac{\{f_{u2,j} - f_2(g, a_{\min}, M_{\min}, r_{\min})\}^2}{\sigma_{f_{u2},j}^2}, \quad (23)$$

where $f_{u1,j}$ and $f_{u2,j}$ are respectively the observed upper and lower HFQPOs for the j^{th} source while f_1 and f_2 are the theoretical model dependent QPO frequencies. The errors in the observed HFQPOs are denoted by $\sigma_{f_{u1},j}$ and $\sigma_{f_{u2},j}$ also mentioned in [Table 1](#) and j runs from 1 to 5. We note from [Table 2](#) that the mathematical expressions for the theoretical QPO frequencies f_1 and f_2 depend on the orbital frequency and the epicyclic frequencies which are functions of the metric parameters g , a , M and the emission radius r_{em} . We however wish to determine the most favored value of g from the QPO observations and hence minimize χ^2 only with respect to g . This requires us to divide the total number of parameters into two classes [94], namely, (a) the “interesting parameters” (in our case g), which are obtained from χ^2 minimization and (b) the “uninteresting parameters” (here a , M and r_{em}), which are also obtained from χ^2 minimization for various fixed values of the “interesting parameters”.

In order to extract the observationally favored value of g , we vary the mass of a chosen source within the error bar mentioned in [Table 1](#) (i.e., $(M_{BH} - \Delta M_{BH}) \leq M_{BH} \leq (M_{BH} + \Delta M_{BH})$), the emission radius between $r_{ms}(g, a) \leq r_{em} \leq r_{ms}(g, a) + 20r_g$ and its spin between the maximally allowed prograde and retrograde values for the chosen g and calculate χ^2 as mentioned in [Eq. \(23\)](#) considering a given model from [Table 2](#). The values of mass, r_{em} and spin for which χ^2 minimizes (denoted by χ_m^2) for the chosen source are represented by M_{\min} , r_{\min} and a_{\min} . We next compute M_{\min} , r_{\min} and a_{\min} and hence χ_m^2 for the remaining sources in [Table 1](#) for the same QPO model, keeping g fixed. We repeat the above procedure for other values of g such that $0 \leq g \leq 0.55$. This enables us to obtain the variation of χ_m^2 with g for the chosen QPO model. The value of g where χ_m^2 minimizes gives us the observationally favored magnitude of g within the domain of the chosen QPO model. The corresponding value of χ_m^2 is denoted by χ_{min}^2 .

The confidence intervals (i.e., $\Delta\chi^2$ from χ^2_{\min}) associated with 68%, 90% and 99% confidence levels are equal to 1, 2.71 and 6.63 [94]. The variation of χ^2 with g for each of the QPO models is shown in Fig. 1 and Fig. 2. Certain QPO models like RPM can also address the low-frequency QPO observed in GRO J1655-40, in which case the form of χ^2 is given by,

$$\chi^2(g) = \sum_j \frac{\{f_{u1,j} - f_1(g, a_{\min}, M_{\min}, r_{\min})\}^2}{\sigma_{f_{u1,j}}^2} + \sum_j \frac{\{f_{u2,j} - f_2(g, a_{\min}, M_{\min}, r_{\min})\}^2}{\sigma_{f_{u2,j}}^2} + \frac{\{f_{L,GRO} - f_3(g, a_{\min}, M_{\min}, r_{\min})\}^2}{\sigma_{f_{L,GRO}}^2}. \quad (24)$$

From the figures it is evident that all the QPO models considered here prefer the general relativistic scenario, since the χ^2 minimizes for $g = 0$.

As mentioned earlier we do not provide independent estimates of mass for the given sources, therefore, the value of M_{\min} corresponding to the most favored g lies somewhere within the error bars mentioned in Table 1. The observationally favored values of BH mass from each of the QPO models are reported in Table 3. We however provide independent estimates of spin from the present analysis since (i) the earlier measurements of spin are based on Kerr geometry, while in our case we are considering Bardeen spacetime and (ii) there exist huge disparity in the spin estimates for the same source (e.g., GRO J1655-40 [56]) when different methods of spin measurements are used assuming general relativity. In Table 4 we report the observationally favored values of spin from the present analysis corresponding to $g = 0$.

We note from Table 4 that previous estimates of spin for sources like GRO J1655-40, GRS 1915+105 and Sgr A* assuming Kerr spacetime exhibit a lot of discrepancy, e.g., for the source GRS 1915+105 the Fe-line method gives a spin $a \sim 0.6 - 0.98$ [103] while the Continuum Fitting Method itself yields maximal ($a \sim 0.98$ [97]) as well as intermediate spin ($a \sim 0.7$ [101]). When revised mass and inclination for this source is considered the spin of GRS 1915+105 turns out to be $0.4 < a < 0.98$. Our results assuming KRM1 and PRM are in best agreement with previous studies [97, 103, 105] (evident from Column 4 of Table 4). For the source GRO J1655-40, assuming Fe-line method the spin turns out to be $0.94 < a < 0.98$ [100], from the Continuum-Fitting method the spin of GRO J1655-40 is $0.65 < a < 0.75$ [95] while from QPO related observations and assuming RPM the spin is given by $a = 0.290 \pm 0.003$ [56]. We note that our spin estimates based on FRM1 and KRM2 are consistent with that of previous spin measurements assuming RPM. Further, the spin of the source that we have obtained assuming PRM and KRM1 are consistent with the results assuming the Fe-line method [100]. The other QPO models however yield spin values which are different from earlier measurements. When we consider the source XTE J1550-564, the Fe-line method yields $a = 0.55^{+0.15}_{-0.22}$ [96] while the Continuum Fitting method gives a spin in the range $-0.11 < a < 0.71$. Our results assuming most of the QPO models are in agreement with previous results, except PRM and KRM1 (see e.g., third column of Table 4). For the source H1743-322 the upper bound on spin turns out to be $a < 0.92$ (with 99.7% confidence) while $a = 0.2 \pm 0.3$ (with 68% confidence) when the Continuum-Fitting method is used [98]. Once again apart from PRM and KRM1 all the other QPO models yield results consistent with earlier measurements. The spin of Sgr A* is obtained from its radio spectrum [99, 102, 107]. Due to the difficulties in modelling the radio spectrum of Sgr A*, there exist a lot of discrepancy in its spin estimates e.g. $a \sim 0.9$ [99], $a \sim 0.5$ [102]. By studying the motion of S2 stars near Sgr A* one obtains $a \lesssim 0.1$ [106] while from the X-ray light curve of Sgr A* one infers a maximal spin for this object ($a = 0.9959 \pm 0.0005$) [104]. Our analysis reveals that the source has a high spin from all the QPO models ($a \geq 0.8$ sixth column of Table 4) which is consistent with [99, 104].

In Fig. 1 and Fig. 2 we plot χ^2 as a function of the magnetic monopole charge parameter g for the QPO models discussed in the last section. In particular Fig. 1 depicts the variation of χ^2 with g for:

Comparison of mass estimates (in M_{\odot})	GRO J1655 – 40	XTE J1550 – 564	GRS 1915 + 105	H 1743 + 322	Sgr A*
Previous constraints	5.4 ± 0.3 [55]	9.1 ± 0.61 [57]	$12.4_{-1.8}^{+2.0}$ [58]	8.0 – 14.07 [59–61]	$(3.5 – 4.9) \times 10^{-3}$ [62, 63]
RPM	5.13 ($g \sim 0$)	9.3 ($g \sim 0$)	13.99 ($g \sim 0$)	12.06 ($g \sim 0$)	4.0×10^6 ($g \sim 0$)
TDM	5.33 ($g \sim 0$)	9.13 ($g \sim 0$)	12.12 ($g \sim 0$)	10.73 ($g \sim 0$)	3.5×10^6 ($g \sim 0$)
PRM	5.17 ($g \sim 0$)	9.63 ($g \sim 0$)	13.75 ($g \sim 0$)	9.39 ($g \sim 0$)	3.5×10^6 ($g \sim 0$)
FRM1	5.2 ($g \sim 0$)	8.51 ($g \sim 0$)	13.2 ($g \sim 0$)	12.57 ($g \sim 0$)	3.5×10^6 ($g \sim 0$)
FRM2	5.33 ($g \sim 0$)	9.27 ($g \sim 0$)	11.42 ($g \sim 0$)	9.28 ($g \sim 0$)	3.6×10^6 ($g \sim 0$)
KRM1	5.17($g \sim 0$)	8.49($g \sim 0$)	12.13($g \sim 0$)	8.0($g \sim 0$)	3.5×10^6 ($g \sim 0$)
KRM2	5.36 ($g \sim 0$)	8.94 ($g \sim 0$)	14.1 ($g \sim 0$)	13.08 ($g \sim 0$)	4.8×10^6 ($g \sim 0$)
KRM3	5.67 ($g \sim 0$)	9.65 ($g \sim 0$)	12.71 ($g \sim 0$)	10.33 ($g \sim 0$)	4.2×10^6 ($g \sim 0$)
WDOM	5.34 ($g \sim 0$)	9.34 ($g \sim 0$)	13.86 ($g \sim 0$)	11.31 ($g \sim 0$)	3.5×10^6 ($g \sim 0$)
NADO1	5.15 ($g \sim 0$)	9.53 ($g \sim 0$)	12.4 ($g \sim 0$)	11.13 ($g \sim 0$)	3.5×10^6 ($g \sim 0$)
NADO2	5.43 ($g \sim 0$)	9.22 ($g \sim 0$)	14.04 ($g \sim 0$)	14.0 ($g \sim 0$)	4×10^6 ($g \sim 0$)

Table 3: In the above table we report the mass estimates of the BH sources considered in Table 1 obtained from χ^2 minimization. These are compared with earlier estimates.

(i) Relativistic Precession Model (RPM), (ii) Tidal Disruption Model (TDM), (iii) Parametric Resonance Model (PRM), (iv) 3:1 Forced Resonance Model (FRM1) and (v) 2:1 Forced Resonance Model (FRM2) while Fig. 2 shows the variation of χ^2 with g for (i) Keplerian Resonance Model 1 (KRM1), (ii) Keplerian Resonance Model 2 (KRM2), (iii) Keplerian Resonance Model 3 (KRM3) (iv) Warped Disc Oscillation Model (WDOM) (v) Non-axisymmetric Disc Oscillation Model 1 (NADO1) and (vi) Non-axisymmetric Disc Oscillation Model 2 (NADO2). The value of g where χ^2 minimizes is denoted by g_{min} and is the one favoured by observations. For each of the QPO models we plot the $1 - \sigma$, $2 - \sigma$ and $3 - \sigma$ confidence intervals which are denoted by $\chi^2 = \chi_{min}^2 + 1$, $\chi^2 = \chi_{min}^2 + 2.71$ and $\chi^2 = \chi_{min}^2 + 6.63$, respectively. These are plotted with black, blue and magenta dashed lines in Fig. 1 and Fig. 2.

We note from Fig. 1 and Fig. 2 that all the eleven QPO models favor the Kerr scenario in general relativity i.e. $g = 0$. In fact the two most widely used QPO models PRM and RPM can establish very

Comparison of spin estimates	GRO J1655 – 40	XTE J1550 – 564	GRS 1915 + 105	H 1743 + 322	Sgr A*
Previous constraints	$a \sim 0.65 - 0.75$ [95] $a \sim 0.94 - 0.98$ [100] $a = 0.29 \pm 0.003$ [56]	$-0.11 < a < 0.71$ [96] $a = 0.55^{+0.15}_{-0.22}$ [96]	$a \sim 0.98$ [97] $a \sim 0.7$ [101] $a \sim 0.6 - 0.98$ [103] $a \sim 0.4 - 0.98$ [105]	$a = 0.2 \pm 0.3$ [98]	$a \sim 0.92$ [99] $a \sim 0.5$ [102] $a = 0.9959 \pm 0.0005$ [104] $a \sim 0.1$ [106]
RPM	0.3 ($g \sim 0$)	0.4 ($g \sim 0$)	0.3 ($g \sim 0$)	0.5 ($g \sim 0$)	0.97 ($g \sim 0$)
TDM	0.1 ($g \sim 0$)	0.23 ($g \sim 0$)	-0.1 ($g \sim 0$)	0.2 ($g \sim 0$)	0.99 ($g \sim 0$)
PRM	0.9 ($g \sim 0$)	0.95 ($g \sim 0$)	0.9 ($g \sim 0$)	0.92 ($g \sim 0$)	0.99 ($g \sim 0$)
FRM1	0.3 ($g \sim 0$)	0.34 ($g \sim 0$)	0.26 ($g \sim 0$)	0.6 ($g \sim 0$)	0.97 ($g \sim 0$)
FRM2	0.1 ($g \sim 0$)	0.25 ($g \sim 0$)	-0.2 ($g \sim 0$)	0.0 ($g \sim 0$)	0.97 ($g \sim 0$)
KRM1	0.99 ($g \sim 0$)	0.99 ($g \sim 0$)	0.97 ($g \sim 0$)	0.99 ($g \sim 0$)	0.99 ($g \sim 0$)
KRM2	0.32 ($g \sim 0$)	0.36 ($g \sim 0$)	0.32 ($g \sim 0$)	0.6 ($g \sim 0$)	0.97 ($g \sim 0$)
KRM3	0.22 ($g \sim 0$)	0.3 ($g \sim 0$)	0.0 ($g \sim 0$)	0.22 ($g \sim 0$)	0.99 ($g \sim 0$)
WDOM	0.1 ($g \sim 0$)	0.26 ($g \sim 0$)	0.1 ($g \sim 0$)	0.26 ($g \sim 0$)	0.99 ($g \sim 0$)
NADO1	0.36 ($g \sim 0$)	0.6 ($g \sim 0$)	0.22 ($g \sim 0$)	0.6 ($g \sim 0$)	0.99 ($g \sim 0$)
NADO2	0.25 ($g \sim 0$)	0.31 ($g \sim 0$)	0.24 ($g \sim 0$)	0.5 ($g \sim 0$)	0.8 ($g \sim 0$)

Table 4: In the above table we report the spin estimates of the BH sources considered in Table 1 obtained from χ^2 minimization. The spin measurements obtained from earlier estimates are also reported.

strong constraints on the monopole charge parameter g , i.e., these models rule out $g \gtrsim 0.03$ outside 99% confidence interval. Interestingly, for RPM, the χ^2 minimizes for $g \simeq 0$ as well $g \simeq 0.25$. We consider $g \simeq 0$ as the global minima and compute the $\Delta\chi^2$ accordingly. It may be important to note that even if we consider χ^2_{min} corresponding to $g \simeq 0.25$ the bounds on the monopole charge parameter turns out to be very stringent when RPM is considered and like all the other QPO models very high values of g seem to be disfavored from observations associated with QPOs. Interestingly, our present result is in agreement with our previous findings where we compare the theoretical spectrum from the accretion disk with the optical observations of quasars and note that the Kerr scenario is more favored compared to the Bardeen black holes [108].

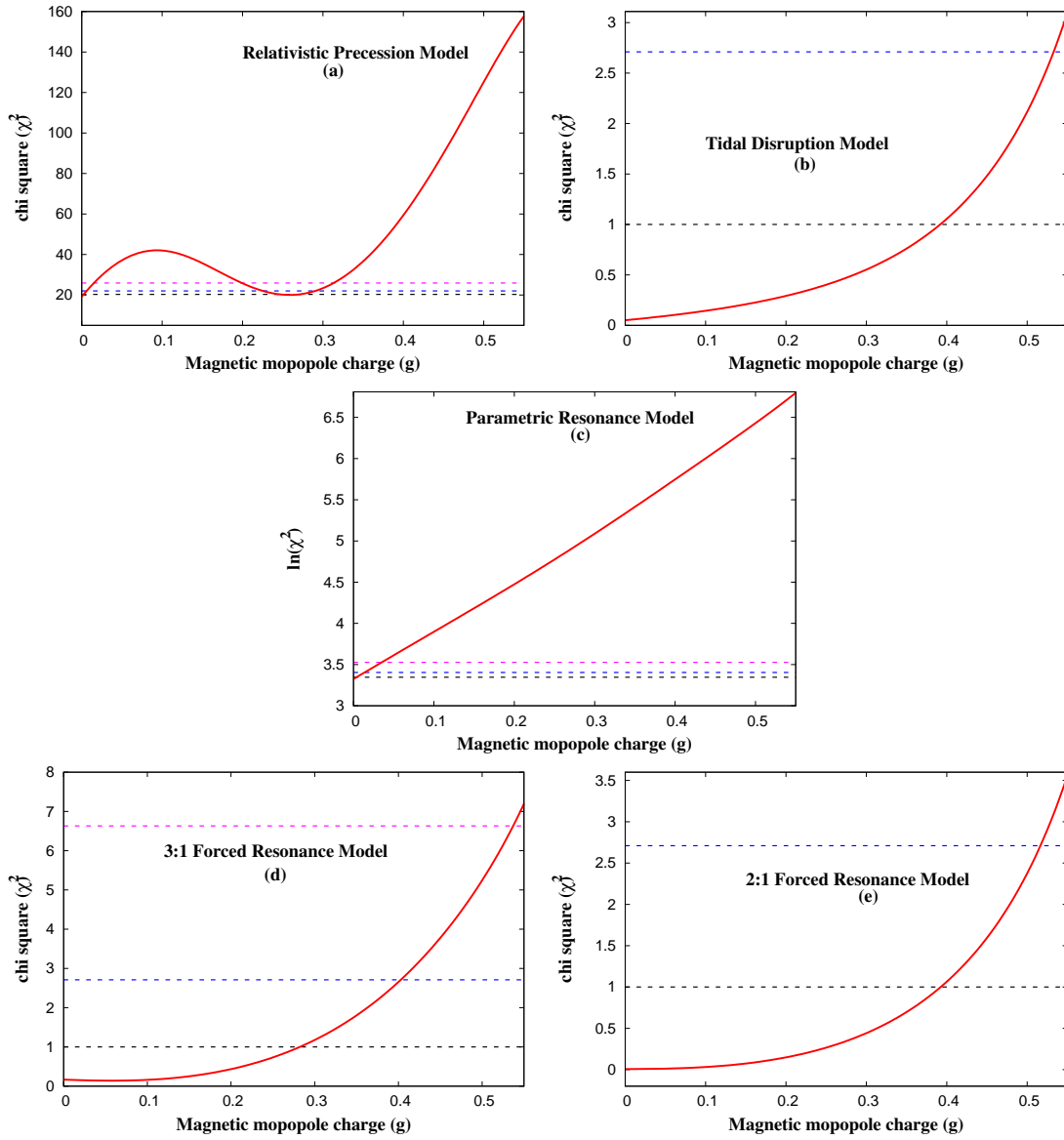


Figure 1: In this figure we plot the variation of χ^2 with g assuming the following QPO models: (a) Relativistic Precession Model (RPM), (b) Tidal Disruption Model (TDM), (c) Parametric Resonance Model (PRM), (d) 3:1 Forced Resonance Model (FRM1) and (e) 2:1 Forced Resonance Model (FRM2). χ^2 minimizes for $g = 0$ for all the above models indicating that the Kerr scenario in general relativity is more favored compared to Bardeen rotating black holes.

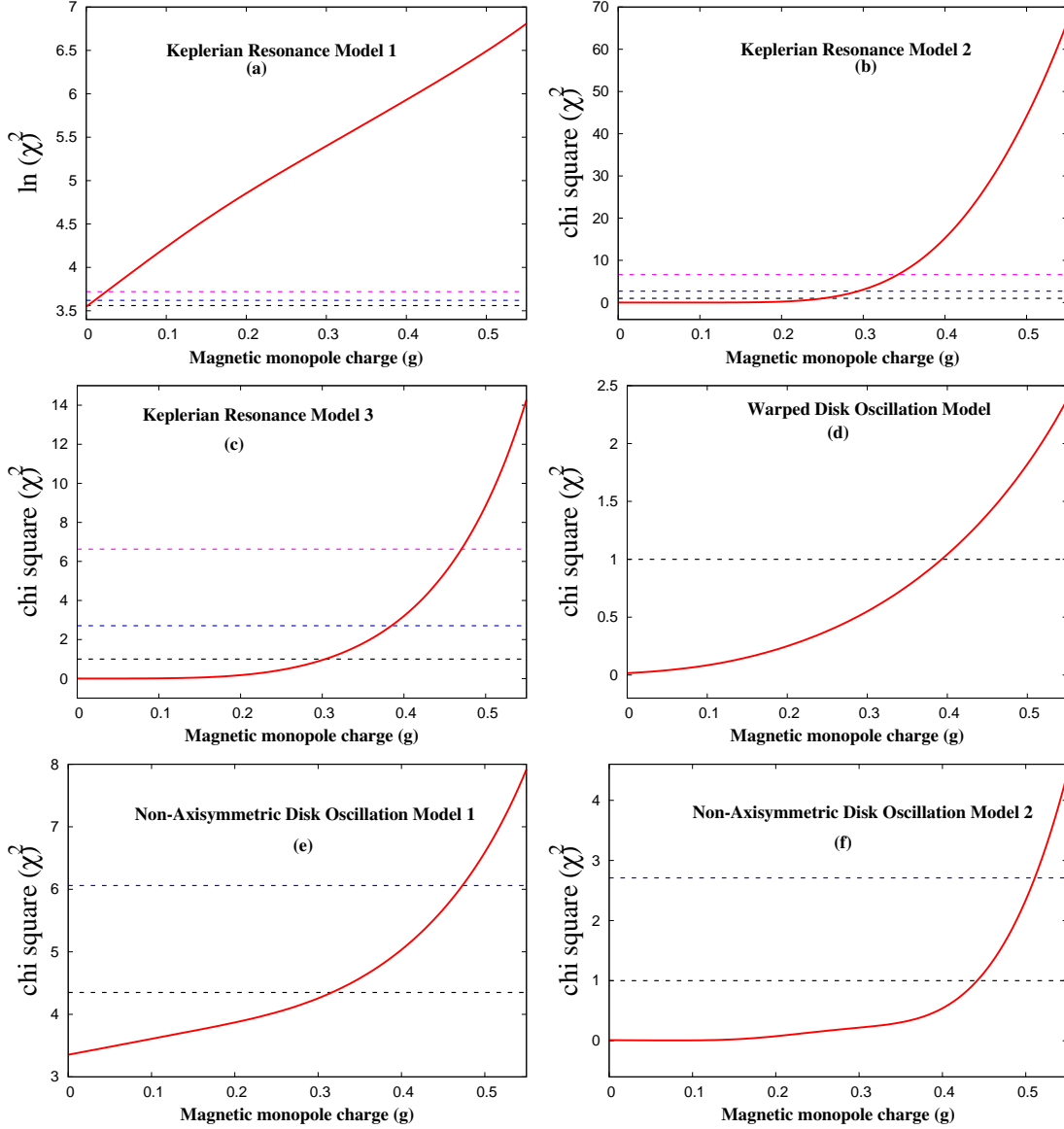


Figure 2: The figure above depicts χ^2 versus g assuming the following models: (a) Keplerian Resonance Model 1, (b) Keplerian Resonance Model 2, (c) Keplerian Resonance Model 3, (d) Warped Disk Oscillation Model, (e) Non-axisymmetric Disc Oscillation Model 1 and (f) Non-axisymmetric Disc Oscillation Model. Here also χ^2 minimizes for $g = 0$ consistent with our earlier findings with the previous models.

6 Concluding Remarks

In this paper we study the signatures of magnetic monopole charge from the observed quasi-periodic oscillations (QPOs) in black holes. Such black holes (known as Bardeen black holes in the literature) are interesting as they can evade the $r = 0$ singularity present in general relativistic black holes. Astrophysical observations, e.g., the broadened and skewed iron-line, the continuum spectrum, the black hole shadow and the quasi-periodic oscillations can be used to extract information regarding the nature of the background spacetime. In this regard, it may be important to note that QPOs and the black hole shadow are cleaner probes to the background spacetime as these are not so much dependent on the complex physics associated with the accretion flow. The role of the magnetic monopole charge on the black hole shadow has been investigated in [109]. In this paper we aim to investigate the role of the magnetic monopole charge in explaining the observed quasi-periodic oscillations in black holes.

Various models have been proposed in the literature to explain the observed QPO frequencies which are dependent on the epicyclic motion of test particles and hence on the background metric. We calculate the theoretical model dependent QPO frequencies in the Bardeen background which in turn are compared with the available observations. By performing a χ^2 analysis between the theoretical and the observed QPO frequencies we arrive at the conclusion that the Kerr scenario in general relativity is more favored than black holes with a monopole charge. Interestingly, this result more or less holds good for all the eleven QPO models considered here. In particular, models like PRM, RPM and KRM1 establish very strong constraints on the magnitude of the magnetic monopole charge such that $g \gtrsim 0.03$ is outside 99% confidence interval. This result is in agreement with our previous findings where we derive the theoretical spectrum from the accretion disk and compare it with the optical observations of quasars and note that the Kerr scenario is more favored compared to the black holes with a magnetic monopole charge. However, the Kerr metric turns out to be black hole solution of several alternative gravity models [] and hence our present result does not uniquely favor the general relativistic scenario compared to other modified gravity theories.

Before concluding we mention some of the limitations of our present analysis. First, our results are model dependent, i.e. the physical mechanism giving rise to the QPOs is not very clearly understood such that despite observing HFQPOs for decades there exist no common consensus regarding the preferred choice of the QPO model that best describes the observations. In fact, it may as well happen that some black hole-accretion disk (BH-AD) systems are described by e.g. PRM while there may be other BH-AD systems which are best described by RPM and so on. Second, our observational sample is small since not many black holes exhibit HFQPOs in their power spectrum. A larger observational sample leads to improved statistics and hence can establish much stronger constraints on the monopole charge parameter g . Finally, the available data is not very precise and with the launch of the ESA (European Space Agency) X-ray mission LOFT (Large Observatory for X-ray Timing) one can expect an improvement in the precision by an order of magnitude which in turn will enhance the scope to investigate the QPO phenomenology in near future.

Acknowledgements

The author acknowledges Sumanta Chakraborty and Soumitra SenGupta for insightful discussion during the course of this work.

References

- [1] C. M. Will, “Was Einstein right?,” *Annalen Phys.* **15** (2005) 19–33, [arXiv:gr-qc/0504086 \[gr-qc\]](#). [Annalen Phys.518,19(2006)].
- [2] C. M. Will, *Theory and experiment in gravitational physics*. 1993.
- [3] C. M. Will, “The Confrontation between general relativity and experiment,” *Living Rev. Rel.* **9** (2006) 3, [arXiv:gr-qc/0510072 \[gr-qc\]](#).
- [4] E. Berti *et al.*, “Testing General Relativity with Present and Future Astrophysical Observations,” *Class. Quant. Grav.* **32** (2015) 243001, [arXiv:1501.07274 \[gr-qc\]](#).
- [5] **Event Horizon Telescope** Collaboration, V. L. Fish, K. Akiyama, K. L. Bouman, A. A. Chael, M. D. Johnson, S. S. Doeleman, L. Blackburn, J. F. C. Wardle, and W. T. Freeman, “Observing — and Imaging — Active Galactic Nuclei with the Event Horizon Telescope,” *Galaxies* **4** no. 4, (2016) 54, [arXiv:1607.03034 \[astro-ph.IM\]](#).
- [6] **Event Horizon Telescope** Collaboration, K. Akiyama *et al.*, “First M87 Event Horizon Telescope Results. I. The Shadow of the Supermassive Black Hole,” *Astrophys. J.* **875** no. 1, (2019) L1, [arXiv:1906.11238 \[astro-ph.GA\]](#).
- [7] **Event Horizon Telescope** Collaboration, K. Akiyama *et al.*, “First M87 Event Horizon Telescope Results. II. Array and Instrumentation,” *Astrophys. J.* **875** no. 1, (2019) L2, [arXiv:1906.11239 \[astro-ph.IM\]](#).
- [8] **Event Horizon Telescope** Collaboration, K. Akiyama *et al.*, “First M87 Event Horizon Telescope Results. III. Data Processing and Calibration,” *Astrophys. J.* **875** no. 1, (2019) L3, [arXiv:1906.11240 \[astro-ph.GA\]](#).
- [9] **Event Horizon Telescope** Collaboration, K. Akiyama *et al.*, “First M87 Event Horizon Telescope Results. IV. Imaging the Central Supermassive Black Hole,” *Astrophys. J.* **875** no. 1, (2019) L4, [arXiv:1906.11241 \[astro-ph.GA\]](#).
- [10] **Event Horizon Telescope** Collaboration, K. Akiyama *et al.*, “First M87 Event Horizon Telescope Results. V. Physical Origin of the Asymmetric Ring,” *Astrophys. J.* **875** no. 1, (2019) L5, [arXiv:1906.11242 \[astro-ph.GA\]](#).
- [11] **Event Horizon Telescope** Collaboration, K. Akiyama *et al.*, “First M87 Event Horizon Telescope Results. VI. The Shadow and Mass of the Central Black Hole,” *Astrophys. J.* **875** no. 1, (2019) L6, [arXiv:1906.11243 \[astro-ph.GA\]](#).
- [12] **LIGO Scientific, VIRGO** Collaboration, B. P. Abbott *et al.*, “GW170104: Observation of a 50-Solar-Mass Binary Black Hole Coalescence at Redshift 0.2,” *Phys. Rev. Lett.* **118** no. 22, (2017) 221101, [arXiv:1706.01812 \[gr-qc\]](#). [Erratum: Phys. Rev. Lett.121,no.12,129901(2018)].
- [13] **LIGO Scientific, Virgo** Collaboration, B. P. Abbott *et al.*, “Binary Black Hole Mergers in the first Advanced LIGO Observing Run,” *Phys. Rev.* **X6** no. 4, (2016) 041015, [arXiv:1606.04856 \[gr-qc\]](#). [erratum: Phys. Rev.X8,no.3,039903(2018)].

- [14] **LIGO Scientific, Virgo** Collaboration, B. P. Abbott *et al.*, “GW151226: Observation of Gravitational Waves from a 22-Solar-Mass Binary Black Hole Coalescence,” *Phys. Rev. Lett.* **116** no. 24, (2016) 241103, [arXiv:1606.04855 \[gr-qc\]](#).
- [15] **LIGO Scientific, Virgo** Collaboration, B. P. Abbott *et al.*, “Tests of general relativity with GW150914,” *Phys. Rev. Lett.* **116** no. 22, (2016) 221101, [arXiv:1602.03841 \[gr-qc\]](#). [Erratum: *Phys. Rev. Lett.* 121, no. 12, 129902 (2018)].
- [16] **LIGO Scientific, Virgo** Collaboration, B. P. Abbott *et al.*, “Observation of Gravitational Waves from a Binary Black Hole Merger,” *Phys. Rev. Lett.* **116** no. 6, (2016) 061102, [arXiv:1602.03837 \[gr-qc\]](#).
- [17] M. Milgrom, “A Modification of the Newtonian dynamics: Implications for galaxies,” *Astrophys. J.* **270** (1983) 371–383.
- [18] M. Milgrom and R. H. Sanders, “MOND and the Dearth of dark matter in ordinary elliptical galaxies,” *Astrophys. J.* **599** (2003) L25–L28, [arXiv:astro-ph/0309617 \[astro-ph\]](#).
- [19] J. Bekenstein and M. Milgrom, “Does the missing mass problem signal the breakdown of Newtonian gravity?,” *Astrophys. J.* **286** (1984) 7–14.
- [20] T. Clifton, P. G. Ferreira, A. Padilla, and C. Skordis, “Modified Gravity and Cosmology,” *Phys. Rept.* **513** (2012) 1–189, [arXiv:1106.2476 \[astro-ph.CO\]](#).
- [21] **Supernova Cosmology Project** Collaboration, S. Perlmutter *et al.*, “Measurements of Omega and Lambda from 42 high redshift supernovae,” *Astrophys. J.* **517** (1999) 565–586, [arXiv:astro-ph/9812133 \[astro-ph\]](#).
- [22] **Supernova Search Team** Collaboration, A. G. Riess *et al.*, “Observational evidence from supernovae for an accelerating universe and a cosmological constant,” *Astron. J.* **116** (1998) 1009–1038, [arXiv:astro-ph/9805201 \[astro-ph\]](#).
- [23] R. Penrose, “Gravitational collapse and space-time singularities,” *Phys. Rev. Lett.* **14** (1965) 57–59.
- [24] S. W. Hawking, “Breakdown of Predictability in Gravitational Collapse,” *Phys. Rev.* **D14** (1976) 2460–2473.
- [25] R. M. Wald, *General Relativity*. The University of Chicago Press, 1st ed., 1984.
- [26] D. Christodoulou, “The formation of black holes and singularities in spherically symmetric gravitational collapse,” *Commun. Pure Appl. Math.* **44** no. 3, (1991) 339–373.
- [27] J. M. Bardeen, “Non-singular general-relativistic gravitational collapse,”.
- [28] W. H. G. Lewin and M. van der Klis, *Compact Stellar X-ray Sources*, vol. 39. 2006.
- [29] M. van der Klis, “Millisecond oscillations in x-ray binaries,” *Ann. Rev. Astron. Astrophys.* **38** (2000) 717–760, [arXiv:astro-ph/0001167](#).
- [30] V. F. Shvartsman, “Halos around “Black Holes”.”, *sovast* **15** (Dec., 1971) 377.

- [31] R. A. Syunyaev, “Variability of X Rays from Black Holes with Accretion Disks,,” *sovast* **16** (June, 1973) 941.
- [32] M. Gierliński, M. Middleton, M. Ward, and C. Done, “A periodicity of ~ 1 hour in X-ray emission from the active galaxy RE J1034+396,,” *nat* **455** no. 7211, (Sept., 2008) 369–371.
- [33] G. Torok, “A Possible 3:2 orbital epicyclic resonance in QPOs frequencies of Sgr A*,” *Astron. Astrophys.* **440** (2005) 1, [arXiv:astro-ph/0412500](#).
- [34] B. Aschenbach, “Measuring mass and angular momentum of black holes with high-frequency quasiperiodic oscillations,,” *Astron. Astrophys.* **425** (2004) 1075–1082, [arXiv:astro-ph/0406545](#).
- [35] M. Middleton, C. Done, M. Ward, M. Gierlinski, and N. Schurch, “RE J1034+396: The origin of the soft X-ray excess and QPO,,” *Mon. Not. Roy. Astron. Soc.* **394** (2009) 250, [arXiv:0807.4847 \[astro-ph\]](#).
- [36] C. Jin, C. Done, and M. Ward, “Re-observing the NLS1 Galaxy RE J1034+396. I. the Long-term, Recurrent X-ray QPO with a High Significance,,” *Mon. Not. Roy. Astron. Soc.* **495** (2020) 3538, [arXiv:2005.05857 \[astro-ph.HE\]](#).
- [37] C. Jin, C. Done, and M. Ward, “Re-observing the NLS1 galaxy RE J1034+396 – II. New insights on the soft X-ray excess, QPO, and the analogy with GRS 1915+105,,” *Mon. Not. Roy. Astron. Soc.* **500** no. 2, (2020) 2475–2495, [arXiv:2007.14704 \[astro-ph.HE\]](#).
- [38] L. Stella and M. Vietri, “Lense-Thirring precession and QPOS in low mass x-ray binaries,,” *Astrophys. J. Lett.* **492** (1998) L59, [arXiv:astro-ph/9709085](#).
- [39] L. Stella and M. Vietri, “khz quasiperiodic oscillations in low-mass x-ray binaries as probes of general relativity in the strong-field regime,,” *Phys. Rev. Lett.* **82** (Jan, 1999) 17–20. <https://link.aps.org/doi/10.1103/PhysRevLett.82.17>.
- [40] L. Stella, M. Vietri, and S. M. Morsink, “Correlations in the quasi-periodic oscillation frequencies of low-mass x-ray binaries and the relativistic precession model,,” *The Astrophysical Journal* **524** no. 1, (Oct, 1999) L63–L66. <https://doi.org/10.1086/312291>.
- [41] A. Cadez, M. Calvani, and U. Kostic, “On the tidal evolution of the orbits of low-mass satellites around black holes,,” *Astron. Astrophys.* **487** (2008) 527–532, [arXiv:0809.1783 \[astro-ph\]](#).
- [42] U. Kostic, A. Cadez, M. Calvani, and A. Gomboc, “Tidal effects on small bodies by massive black holes,,” *Astron. Astrophys.* **496** (2009) 307, [arXiv:0901.3447 \[astro-ph.HE\]](#).
- [43] C. Germana, U. Kostic, A. Cadez, and M. Calvani, “Tidal disruption of small satellites orbiting black holes,,” *AIP Conf. Proc.* **1126** no. 1, (2009) 367–369, [arXiv:0902.2134 \[astro-ph.HE\]](#).
- [44] W. Kluzniak and M. A. Abramowicz, “Parametric epicyclic resonance in black hole disks: qpos in micro-quasars,,” [arXiv:astro-ph/0203314](#).
- [45] M. A. Abramowicz, V. Karas, W. Kluzniak, W. H. Lee, and P. Rebusco, “Nonlinear resonance in nearly geodesic motion in low mass x-ray binaries,,” *Publ. Astron. Soc. Jap.* **55** (2003) 466–467, [arXiv:astro-ph/0302183](#).

- [46] P. Rebusco, “Twin peaks kHz QPOs: Mathematics of the 3:2 orbital resonance,” *Publ. Astron. Soc. Jap.* **56** (2004) 553, [arXiv:astro-ph/0403341](#).
- [47] M. A. Nowak, R. V. Wagoner, M. C. Begelman, and D. E. Lehr, “The 67 hz feature in the black hole candidate grs 1915+105 as a possible “diskoseismic” mode,” *Astrophys. J. Lett.* **477** (1997) L91, [arXiv:astro-ph/9612142](#).
- [48] G. Torok, P. Bakala, E. Sramkova, Z. Stuchlik, and M. Urbanec, “On mass-constraints implied by the relativistic precession model of twin-peak quasi-periodic oscillations in Circinus X-1,” *Astrophys. J.* **714** (2010) 748–757, [arXiv:1008.0088](#) [[astro-ph.HE](#)].
- [49] G. Torok, A. Kotrlova, E. Sramkova, and Z. Stuchlik, “Confronting the models of 3:2 quasiperiodic oscillations with the rapid spin of the microquasar GRS 1915+105,” *Astron. Astrophys.* **531** (2011) A59, [arXiv:1103.2438](#) [[astro-ph.HE](#)].
- [50] A. Kotrlová, E. Šrámková, G. Török, K. Goluchová, J. Horák, O. Straub, D. Lancová, Z. Stuchlík, and M. A. Abramowicz, “Models of high-frequency quasi-periodic oscillations and black hole spin estimates in Galactic microquasars,” *Astron. Astrophys.* **643** (2020) A31, [arXiv:2008.12963](#) [[astro-ph.HE](#)].
- [51] S. Kato and J. Fukue, “Trapped Radial Oscillations of Gaseous Disks around a Black Hole,” *Publ. Astron. Soc. Jap.* **32** (1980) 377.
- [52] C. A. Perez, A. S. Silbergleit, R. V. Wagoner, and D. E. Lehr, “Relativistic diskoseismology. 1. Analytical results for ‘gravity modes’,” *Astrophys. J.* **476** (1997) 589–604, [arXiv:astro-ph/9601146](#).
- [53] A. S. Silbergleit, R. V. Wagoner, and M. Ortega-Rodriguez, “Relativistic diskoseismology. 2. Analytical results for C modes,” *Astrophys. J.* **548** (2001) 335–347, [arXiv:astro-ph/0004114](#).
- [54] J. Dexter and O. Blaes, “A model of the steep power law spectra and high-frequency quasi-periodic oscillations in luminous black hole X-ray binaries,” *Mon. Not. Roy. Astron. Soc.* **438** no. 4, (2014) 3352–3357, [arXiv:1312.0941](#) [[astro-ph.HE](#)].
- [55] M. E. Beer and P. Podsiadlowski, “The quiescent light curve and evolutionary state of gro j1655-40,” *Mon. Not. Roy. Astron. Soc.* **331** (2002) 351, [arXiv:astro-ph/0109136](#).
- [56] S. E. Motta, T. M. Belloni, L. Stella, T. Muñoz Darias, and R. Fender, “Precise mass and spin measurements for a stellar-mass black hole through X-ray timing: the case of GRO J1655–40,” *Mon. Not. Roy. Astron. Soc.* **437** no. 3, (2014) 2554–2565, [arXiv:1309.3652](#) [[astro-ph.HE](#)].
- [57] J. A. Orosz, J. F. Steiner, J. E. McClintock, M. A. P. Torres, R. A. Remillard, C. D. Bailyn, and J. M. Miller, “An Improved Dynamical Model for the Microquasar XTE J1550-564,” *Astrophys. J.* **730** (2011) 75, [arXiv:1101.2499](#) [[astro-ph.SR](#)].
- [58] M. J. Reid, J. E. McClintock, J. F. Steiner, D. Steeghs, R. A. Remillard, V. Dhawan, and R. Narayan, “A Parallax Distance to the Microquasar GRS 1915+105 and a Revised Estimate of its Black Hole Mass,” *Astrophys. J.* **796** (2014) 2, [arXiv:1409.2453](#) [[astro-ph.GA](#)].

- [59] G. Pei, S. Nampalliwar, C. Bambi, and M. J. Middleton, “Blandford-Znajek mechanism in black holes in alternative theories of gravity,” *Eur. Phys. J. C* **76** no. 10, (2016) 534, [arXiv:1606.04643 \[gr-qc\]](#).
- [60] A. Bhattacharjee, I. Banerjee, A. Banerjee, D. Debnath, and S. K. Chakrabarti, “The 2004 Outburst of BHC H1743-322: Analysis of spectral and timing properties using the TCAF Solution,” *Mon. Not. Roy. Astron. Soc.* **466** (2017) 1372–1381, [arXiv:1901.00810 \[astro-ph.HE\]](#).
- [61] J. Petri, “A new model for QPOs in accreting black holes: application to the microquasar GRS 1915+105,” *Astrophys. Space Sci.* **318** (2008) 181–186, [arXiv:0809.3115 \[astro-ph\]](#).
- [62] A. M. Ghez *et al.*, “Measuring Distance and Properties of the Milky Way’s Central Supermassive Black Hole with Stellar Orbits,” *Astrophys. J.* **689** (2008) 1044–1062, [arXiv:0808.2870 \[astro-ph\]](#).
- [63] S. Gillessen, F. Eisenhauer, S. Trippe, T. Alexander, R. Genzel, F. Martins, and T. Ott, “Monitoring stellar orbits around the Massive Black Hole in the Galactic Center,” *Astrophys. J.* **692** (2009) 1075–1109, [arXiv:0810.4674 \[astro-ph\]](#).
- [64] Z. Stuchlík and A. Kotrlová, “Orbital resonances in discs around braneworld Kerr black holes,” *Gen. Rel. Grav.* **41** (2009) 1305–1343, [arXiv:0812.5066 \[astro-ph\]](#).
- [65] C. Jin, M. Ward, C. Done, and J. Gelbord, “A combined optical and X-ray study of unobscured type 1 active galactic nuclei - I. Optical spectra and spectral energy distribution modelling,” *mnras* **420** no. 3, (Mar., 2012) 1825–1847, [arXiv:1109.2069 \[astro-ph.HE\]](#).
- [66] B. Czerny, B. You, A. Kurcz, J. Średzińska, K. Hryniewicz, M. Nikolajuk, M. Krupa, J. M. Wang, C. Hu, and P. T. Życki, “The mass of the black hole in RE J1034+396,” *Astron. Astrophys.* **594** (2016) A102, [arXiv:1601.02498 \[astro-ph.GA\]](#).
- [67] K. Chaudhury *et al.*, “Long-term X-ray variability characteristics of the narrow-line Seyfert 1 galaxy RE J1034+396,” *Mon. Not. Roy. Astron. Soc.* **478** no. 4, (2018) 4830–4836, [arXiv:1807.06460 \[astro-ph.HE\]](#).
- [68] M. A. Abramowicz and W. Kluźniak, “A precise determination of black hole spin in GRO J1655-40,” *Astron. Astrophys.* **374** (2001) L19–L20, [arXiv:astro-ph/0105077 \[astro-ph\]](#).
- [69] W. Kluzniak and M. A. Abramowicz, “Strong-Field Gravity and Orbital Resonance in Black Holes and Neutron Stars — kHz Quasi-Periodic Oscillations (QPO),” *Acta Physica Polonica B* **32** no. 11, (Nov., 2001) 3605.
- [70] J. Horak, M. Abramowicz, V. Karas, and W. Kluzniak, “Of NBOs and kHz QPOs: A Low-frequency modulation in resonant oscillations of relativistic accretion disks,” *Publ. Astron. Soc. Jap.* **56** (2004) 819–822, [arXiv:astro-ph/0408090](#).
- [71] G. Török, M. A. Abramowicz, W. Kluźniak, and Z. Stuchlík, “The orbital resonance model for twin peak kHz quasi periodic oscillations in microquasars,” *Astron. Astrophys.* **436** no. 1, (2005) 1–8.
- [72] L. D. Landau and E. M. Lifshitz, *Mechanics*. 1969.

- [73] W. H. Lee, M. A. Abramowicz, and W. Kluźniak, “Resonance in Forced Oscillations of an Accretion Disk and Kilohertz Quasi-periodic Oscillations,” *apjl* **603** no. 2, (Mar., 2004) L93–L96, [arXiv:astro-ph/0402084](#) [astro-ph].
- [74] S. Kato, “Trapping of Non-Axisymmetric g-Mode Oscillations in Thin Relativistic Disks and kHz QPOs,” *PASJ* **53** no. 5, (Oct., 2001) L37–L39.
- [75] M. A. Abramowicz, G. Björnsson, and J. E. Pringle, *Theory of Black Hole Accretion Discs*. 2010.
- [76] L.-X. Li, J. Goodman, and R. Narayan, “Non-axisymmetric g-mode and p-mode instability in a thin accretion disk,” *Astrophys. J.* **593** (2003) 980, [arXiv:astro-ph/0210455](#).
- [77] S. Kato, “Damping and Frequencies of Non-Axisymmetric Trapped g-Mode Oscillations,” *PASJ* **55** (Feb., 2003) 257–265.
- [78] K. Yagi and L. C. Stein, “Black Hole Based Tests of General Relativity,” *Class. Quant. Grav.* **33** no. 5, (2016) 054001, [arXiv:1602.02413](#) [gr-qc].
- [79] S. Kato, “Basic Properties of Thin-Disk Oscillations ¹,” *pasj* **53** no. 1, (Feb., 2001) 1–24.
- [80] S. Kato, “Wave-Warp Resonant Interactions in Relativistic Disks and kHz QPOs,” *pasj* **56** (June, 2004) 559–567.
- [81] S. Kato, “Resonant Excitation of Disk Oscillations by Warps: A Model of kHz QPOs,” *pasj* **56** (Oct., 2004) 905–922, [arXiv:astro-ph/0409051](#) [astro-ph].
- [82] S. Kato, “A Vertical Resonance of g-Mode Oscillations in Warped Disks and QPOs in Low-Mass X-Ray Binaries,” *pasj* **57** (Aug., 2005) 699–703, [arXiv:astro-ph/0507234](#) [astro-ph].
- [83] S. Kato, “Resonant Excitation of Disk Oscillations in Deformed Disks II: A Model of High-Frequency QPOs,” *pasj* **60** (Feb., 2008) 111, [arXiv:0709.2467](#) [astro-ph].
- [84] M. Bursa, M. A. Abramowicz, V. Karas, and W. Kluźniak, “The Upper Kilohertz Quasi-periodic Oscillation: A Gravitationally Lensed Vertical Oscillation,” *apjl* **617** no. 1, (Dec., 2004) L45–L48, [arXiv:astro-ph/0406586](#) [astro-ph].
- [85] M. Bursa, “Global oscillations of a fluid torus as a modulation mechanism for black-hole high-frequency QPOs,” *Astronomische Nachrichten* **326** no. 9, (Nov., 2005) 849–855, [arXiv:astro-ph/0510460](#) [astro-ph].
- [86] M. Bursa, “High-frequency QPOs in GRO J1655-40: Constraints on resonance models by spectral fits,” in *RAGtime 6/7: Workshops on black holes and neutron stars*, S. Hledík and Z. Stuchlík, eds., pp. 39–45. Dec., 2005.
- [87] G. Török, K. Goluchová, J. Horák, E. Šrámková, M. Urbanec, T. Pecháček, and P. Bakala, “Twin peak quasi-periodic oscillations as signature of oscillating cusp torus,” *Mon. Not. Roy. Astron. Soc.* **457** no. 1, (2016) L19–L23, [arXiv:1512.03841](#) [astro-ph.HE].
- [88] E. Sramkova, G. Torok, A. Kotrlova, P. Bakala, M. Abramowicz, Z. Stuchlik, K. Goluchova, and W. Kluźniak, “Black hole spin inferred from 3:2 epicyclic resonance model of high-frequency quasi-periodic oscillations,” *Astron. Astrophys.* **578** (2015) A90, [arXiv:1505.02712](#) [astro-ph.HE].

- [89] J. Horak, “Weak nonlinear coupling between epicyclic modes in slender tori,” *Astron. Astrophys.* **486** (2008) 1, [arXiv:0805.2059 \[astro-ph\]](#).
- [90] Z. Stuchlík and M. Kološ, “Models of quasi-periodic oscillations related to mass and spin of the GRO J1655-40 black hole,” *Astron. Astrophys.* **586** (2016) A130, [arXiv:1603.07366 \[astro-ph.HE\]](#).
- [91] D. Tsang and D. Lai, “Corotational Damping of Diskoseismic C-modes in Black Hole Accretion Discs,” *Mon. Not. Roy. Astron. Soc.* **393** (2009) 992–998, [arXiv:0810.1299 \[astro-ph\]](#).
- [92] W. Fu and D. Lai, “Effects of Magnetic Fields on the Diskoseismic Modes of Accreting Black Holes,” *Astrophys. J.* **690** (2009) 1386–1392, [arXiv:0806.1938 \[astro-ph\]](#).
- [93] W. Fu and D. Lai, “Corotational Instability, Magnetic Resonances and Global Inertial-Acoustic Oscillations in Magnetized Black-Hole Accretion Discs,” *Mon. Not. Roy. Astron. Soc.* **410** (2011) 399, [arXiv:1006.3763 \[astro-ph.HE\]](#).
- [94] Y. Avni, “Energy spectra of X-ray clusters of galaxies,” *Apj* **210** (1976) 642–646.
- [95] R. Shafee, J. E. McClintock, R. Narayan, S. W. Davis, L.-X. Li, and R. A. Remillard, “Estimating the spin of stellar-mass black holes by spectral fitting of the x-ray continuum,” *The Astrophysical Journal* **636** no. 2, (Dec, 2005) L113–L116. <https://doi.org/10.1086/498938>.
- [96] J. F. Steiner, R. C. Reis, J. E. McClintock, R. Narayan, R. A. Remillard, J. A. Orosz, L. Gou, A. C. Fabian, and M. A. P. Torres, “The Spin of the Black Hole Microquasar XTE J1550-564 via the Continuum-Fitting and Fe-Line Methods,” *Mon. Not. Roy. Astron. Soc.* **416** (2011) 941–958, [arXiv:1010.1013 \[astro-ph.HE\]](#).
- [97] J. E. McClintock, R. Shafee, R. Narayan, R. A. Remillard, S. W. Davis, and L.-X. Li, “The Spin of the Near-Extreme Kerr Black Hole GRS 1915+105,” *Astrophys. J.* **652** (2006) 518–539, [arXiv:astro-ph/0606076](#).
- [98] J. F. Steiner, J. E. McClintock, and M. J. Reid, “The Distance, Inclination, and Spin of the Black Hole Microquasar H1743-322,” *Astrophys. J. Lett.* **745** (2012) L7, [arXiv:1111.2388 \[astro-ph.HE\]](#).
- [99] M. Moscibrodzka, C. F. Gammie, J. C. Dolence, H. Shiokawa, and P. K. Leung, “Radiative Models of Sgr A* from GRMHD Simulations,” *Astrophys. J.* **706** (2009) 497–507, [arXiv:0909.5431 \[astro-ph.HE\]](#).
- [100] J. M. Miller, C. S. Reynolds, A. C. Fabian, G. Miniutti, and L. C. Gallo, “Stellar-mass Black Hole Spin Constraints from Disk Reflection and Continuum Modeling,” *Astrophys. J.* **697** (2009) 900–912, [arXiv:0902.2840 \[astro-ph.HE\]](#).
- [101] M. Middleton, C. Done, M. Gierliński, and S. W. Davis, “Black hole spin in GRS 1915+105,” *mnras* **373** no. 3, (Dec., 2006) 1004–1012, [arXiv:astro-ph/0601540 \[astro-ph\]](#).
- [102] R. V. Shcherbakov, R. F. Penna, and J. C. McKinney, “Sagittarius A* Accretion Flow and Black Hole Parameters from General Relativistic Dynamical and Polarized Radiative Modeling,” *Astrophys. J.* **755** (2012) 133, [arXiv:1007.4832 \[astro-ph.HE\]](#).

- [103] J. L. Blum, J. M. Miller, A. C. Fabian, M. C. Miller, J. Homan, M. van der Klis, E. M. Cackett, and R. C. Reis, “Measuring the Spin of GRS 1915+105 with Relativistic Disk Reflection,” *Astrophys. J.* **706** (2009) 60–66, [arXiv:0909.5383 \[astro-ph.HE\]](#).
- [104] B. Aschenbach, “Mass and spin of the Sgr A* supermassive black hole determined from flare lightcurves and flare start times,” *memsai* **81** (Jan., 2010) 319.
- [105] B. S. Mills, S. W. Davis, and M. J. Middleton, “The black hole spin in GRS 1915+105, revisited,” *Astrophys. J.* **914** (2021) 6, [arXiv:2101.11655 \[astro-ph.HE\]](#).
- [106] G. Fragione and A. Loeb, “An upper limit on the spin of SgrA* based on stellar orbits in its vicinity,” *Astrophys. J. Lett.* **901** no. 2, (2020) L32, [arXiv:2008.11734 \[astro-ph.GA\]](#).
- [107] C. S. Reynolds, “The Spin of Supermassive Black Holes,” *Class. Quant. Grav.* **30** (2013) 244004, [arXiv:1307.3246 \[astro-ph.HE\]](#).
- [108] I. Banerjee, V. S. Chawan, B. Mandal, S. K. Sahoo, and S. SenGupta, “Quasar continuum spectrum disfavors black holes with a magnetic monopole charge,” [arXiv:2112.05385 \[gr-qc\]](#).
- [109] R. Kumar and S. G. Ghosh, “Black Hole Parameter Estimation from Its Shadow,” *Astrophys. J.* **892** (2020) 78, [arXiv:1811.01260 \[gr-qc\]](#).